Tissue-Characteristic Expression of Mouse Proteome

Authors

Tian Lu, Liujia Qian, Yuting Xie, Qiushi Zhang, Wei Liu, Weigang Ge, Yi Zhu, Lijia Ma, Cheng Zhang, and Tiannan Guo

Correspondence

malijia@westlake.edu.cn;
zhangcheng@westlake.edu.cn;
guotiannan@westlake.edu.cn

Graphical Abstract

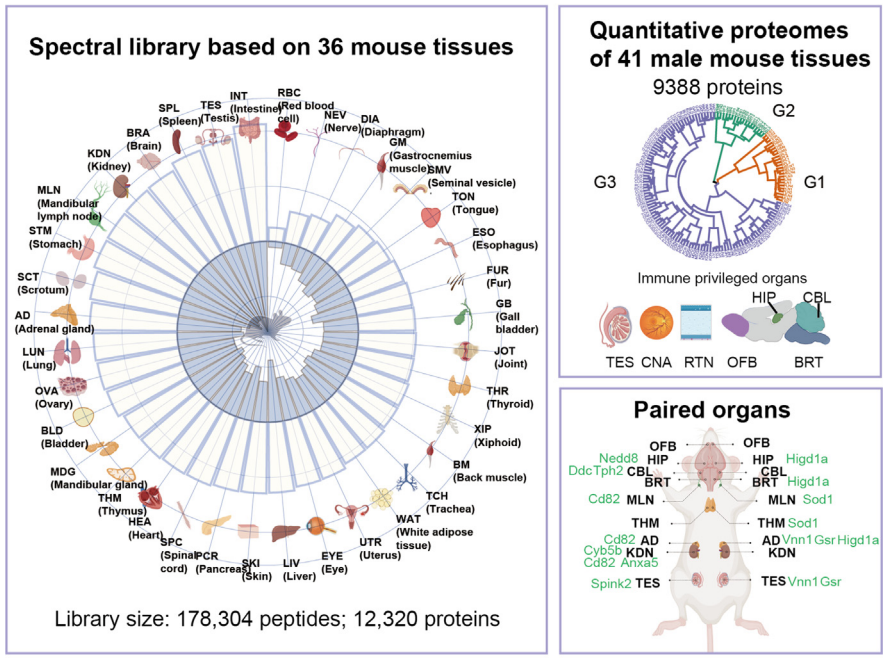

In Brief

We present a quantitative proteomic landscape of 41 mouse tissues and a comprehensive spectral library containing 12,320 proteins. Activation of immunosuppressive pathways and decreased immune activities were found in immune privileged organs. The testis expressed the highest number of tissue-specific proteins. We also found elevated antioxidant enzymes on the left side of multiple organs.

Highlights

- A comprehensive spectral library for 36 mouse tissues containing 12,320 proteins.
- Quantitative proteomics of 41 male mouse tissues characterizes 9388 proteins.
- Immunosuppression in immune privileged organs.
- The testis expressed the highest number of tissue-specific proteins.
- Higher antioxidant enzymes on the left side of multiple paired organs.

2022, Mol Cell Proteomics *21*(*10*), 100408

https://doi.org/10.1016/j.mcpro.2022.100408

Tissue-Characteristic Expression of Mouse Proteome

Tian Lu[1,2,3], Liujia Qian[2,3], Yuting Xie[2,3], Qiushi Zhang[4], Wei Liu[4], Weigang Ge[4], Yi Zhu[2,3], Lijia Ma[1,2,3,*], Cheng Zhang[2,3,*], and Tiannan Guo[1,2,3,*]

The mouse is a valuable model organism for biomedical research. Here, we established a comprehensive spectral library and the data-independent acquisition–based quantitative proteome maps for 41 mouse organs, including some rarely reported organs such as the cornea, retina, and nine paired organs. The mouse spectral library contained 178,304 peptides from 12,320 proteins, including 1678 proteins not reported in previous mouse spectral libraries. Our data suggested that organs from the nervous system and immune system expressed the most distinct proteome compared with other organs. We also found characteristic protein expression of immune-privileged organs, which may help understanding possible immune rejection after organ transplantation. Each tissue type expressed characteristic high-abundance proteins related to its physiological functions. We also uncovered some tissue-specific proteins which have not been reported previously. The testis expressed highest number of tissue-specific proteins. By comparison of nine paired organs including kidneys, testes, and adrenal glands, we found left organs exhibited higher levels of antioxidant enzymes. We also observed expression asymmetry for proteins related to the apoptotic process, tumor suppression, and organ functions between the left and right sides. This study provides a comprehensive spectral library and a quantitative proteome resource for mouse studies.

The mouse has long served as a key model organism for the study of human biology and diseases. The genome and transcriptome of multiple mouse tissues have been characterized (1–4). High spatial resolution transcriptomics studies have uncovered a high degree of heterogeneity among tissue types (3, 4). Proteins are the gears of life activities and the main drug targets. Mass spectrometry (MS) is a powerful tool for characterizing proteomes (5).

Data-dependent acquisition (DDA)-MS could be used to comprehensively catalog proteins expressed in a sample. A few studies have tried to investigate protein expression in multiple mouse tissues with DDA-MS. In 2006, Kislinger *et al.* (6) characterized 4768 proteins in four major subcellular compartments in six organs using DDA-MS. Four years later, a tissue-specific atlas of mouse protein phosphorylation and expression based on nine mouse tissues was reported (7). This study characterized 12,039 proteins, including 6296 phosphoproteins. Recently, Skinnider *et al.* (8) mapped the interactomes of seven mouse tissues based on size-exclusion chromatography and protein correlation profiling–stable isotope labeling by amino acids in cell culture (SILAC). Altogether, they reported 123,000 protein interactions among 7225 proteins. In 2013, Geiger *et al.* (9) reported a SILAC-based quantitative landscape of 7349 proteins in 28 mouse tissues based on a FASTA database containing 59,345 curated and predicted mouse protein sequences. During the review of this paper, the Kuster group published a DDA-MS–based proteomic investigation of 41 mouse tissues, covering 17,883 proteins, thousands of isoforms, and 50,000 phosphorylation sites based on a FASTA database containing 61,307 curated and predicted mouse protein sequences (10).

Data-independent acquisition (DIA) is widely used in label-free quantification of large sample sets, exhibiting satisfactory quantitative reproducibility, proteomic depth, and throughput (11, 12). An enhanced DIA method, called Pulse-DIA (13), was recently developed with improved proteomic depth by taking advantage of gas phase separation and multiple injection. Both library-free and library-based methods have been developed for analyzing DIA data (12), but tissue-specific library is beneficial in most cases (14–16). Moreover, targeted validation of selected proteins and peptides relies on the availability of spectral libraries. Two SWATH libraries have been published with more than 10,000 proteins (17, 18). However, there is still no comprehensive DIA-based quantitative proteomic investigations of various mouse tissues. In this study, we generated a comprehensive mouse spectral

From the [1]School of Life Sciences, Fudan University, Shanghai, China; [2]Key Laboratory of Structural Biology of Zhejiang Province, School of Life Sciences, Westlake University, Hangzhou, Zhejiang, China; [3]Westlake Intelligent Biomarker Discovery Lab, Westlake Laboratory of Life Sciences and Biomedicine, Hangzhou, Zhejiang, China; [4]Westlake Omics (Hangzhou) Biotechnology Co, Ltd, Hangzhou, China
*For correspondence: Tiannan Guo, guotiannan@westlake.edu.cn; Lijia Ma, malijia@westlake.edu.cn; Cheng Zhang, zhangcheng@westlake.edu.cn.

https://doi.org/10.1016/j.mcpro.2022.100408

library containing 12,320 proteins from 36 tissues based on a curated mouse protein sequence FASTA file containing 16,935 entries. We also reported expression of 9388 proteins in 41 organs from four male mice and nine paired organs from 12 male mice. The unique data resource permits unprecedented exploration of mouse proteome.

EXPERIMENTAL PROCEDURES

Tissue Dissection

Eight-week-old female and male C57BL/6 mice were anesthetized by intraperitoneal injection of pentobarbital sodium followed by perfusion with normal saline to minimize potential contamination of blood proteins to organs. The white fat attached to some organs, such as kidney, intestine, and stomach, among others, were carefully removed to the maximum extent before protein extraction. Most organs, such as heart, lungs, liver, and among others, are clearly delimited, so the probability of contamination was relatively small. For different brain regions and different regions of the intestines, we selected tissues that could be distinguished by the naked eye. For example, hippocampus could be peeled intact from the brain. Cecum has a very different morphology from other regions. For spectral library generation, an average of 15 mg tissue weight was required for 36 tissue types, which was closely related to the protein extraction rate of each tissue (supplemental Table S1). As for the quantitative mouse proteome analysis, an average of 1.5 mg tissue weight was collected, and the abbreviations for each organ can be found in supplemental Table S2. All surgical instruments were washed after collection of each organ with saline to avoid potential contamination. These operations were performed in a 4 °C environment, and samples were stored in −80 °C until protein extraction. These experiments were approved by the Laboratory Animal Resources Center, Westlake University.

Pressure Cycling Technology–Assisted Sample Preparation

All samples were lysed first with the assistance of pressure cycling technology (PCT) as previously described (11, 19). Briefly, tissues were lysed in 30 μl of denaturing buffer containing 6 M urea, 2 M thiourea, and 100 mM ammonium bicarbonate in PCT. The applied program contained 90 oscillating cycles, with each cycle consisting of 25 s of high pressure at 45,000 psi and 10 s of ambient pressure. Then, the extracted proteins were reduced first with 10 mM Tris (2-carboxyethyl) phosphine at 25 °C for 30 min, followed by alkylation with 20 mM iodoacetamide at 25 °C in the dark for 30 min. Then, the samples for library generation were subject to in-solution digestion with trypsin (Hualishi, enzyme-to-substrate ratio, 1:100, twice). Samples for PulseDIA analysis were digested with Lys-C (Hualishi; enzyme-to-substrate ratio, 1:40) using PCT (20,000 psi, 50 s and ambient pressure, 10 s each cycle, 45 cycles), followed by trypsin (Hualishi, enzyme-to-substrate ratio, 1:50) digestion in the Barocycler (20,000 psi, 50 s and 10 s ambient pressure, 90 cycles). Digestion was stopped by adjusting pH to 2 to 3 with trifluoroacetic acid, and the peptides were cleaned with C18 cartridges (17–170 μg capacity, Part No. HEM S18V, MA).

Strong Cation Exchange Fractionation for Generating Spectral Library

Thirty-six peptide samples for spectral library generation were fractionated by strong cation exchange (SCX) solid-phase extraction cartridge (Thermo Scientific, # 60108-421) into six fractions according to the manufacturer's protocol. Briefly, vacuum-dried peptides were dissolved in 5 mM KH_2PO_4/25% ACN (pH = 3.0), then loaded onto the well-conditioned SCX solid-phase extraction cartridge. KCl concentrations in 5 mM KH_2PO_4/25% ACN for the six elution buffers were 50 mM, 100 mM, 150 mM, 250 mM, 350 mM, and 500 mM, respectively. After dried in the vacuum and desalted by C18, each fraction was redissolved, and iRT calibration standard peptides was spiked in before liquid chromatography (LC)-MS analysis.

LC-MS Analysis

LC-MS measurements were performed on a nanoEasy-nLC 1200 System (Thermo Fisher Scientific) (precolumn, 20 mm*75 μm i.d. with 3 μm100 Å C18; analytical column, 150 mm*75 μm i.d. with 1.9 μm 120 Å C18) coupled to a Q Exactive HF-X hybrid Quadrupole-Orbitrap mass spectrometer (Thermo Fisher Scientific) for library generation and the PulseDIA data of female mouse tissues. The data of samples for the following quantitative analysis and proteomic laterality study were collected on a Q Exactive HF hybrid Quadrupole-Orbitrap mass spectrometer (Thermo Fisher Scientific) with the same settings of LC system. For samples of library generation, peptides were separated by a 90-min LC gradient (from 3 to 28% buffer B; buffer A: 98% H2O, 2% ACN, 0.1% FA, buffer B: 98% ACN, 2% H2O and 0.1% FA). MS1 was performed within a m/z range of 390 to 1210 with resolution at 60,000, an AGC target of 3e6, and a maximum ion injection time of 80 ms. Then, the top 20 precursors from each MS scan were selected to be fragmented and measured at 30,000 resolution with an AGC target of 1e5 and a maximum ion injection time of 100 ms. Samples for the following analysis underwent a two-part PulseDIA method (13). Briefly, peptides for the female mouse data were injected and separated twice using a 30-min LC gradient (from 3 to 28% buffer B), while peptides for the data of the following quantitative analysis and proteomic laterality study were injected and separated twice using a 45-min LC gradient (from 3 to 28% buffer B). The m/z range of MS1 was 390 to 1210 at 60,000 resolution, with an AGC target of 3e6 and a maximum ion injection time of 80 ms. Isolation windows for the two parts were as followings (m/z): part1: 399.5 to 410.5, 419.5 to 430.5, 439.5 to 450.5, 459.5 to 470.5, 479.5 to 490.5, 499.5 to 510.5, 519.5 to 530.5, 539.5 to 550.5, 559.5 to 570.5, 579.5 to 590.5, 599.5 to 610.5, 619.5 to 630.5, 639.5 to 650.5, 659.5 to 670.5, 679.5 to 690.5, 699.5 to 710.5, 719.5 to 730.5, 739.5 to 750.5, 759.5 to 770.5, 779.5 to 790.5, 799.5 to 830.5, 859.5 to 900.5, 939.5 to 1000.5, 1059.5 to 1130.5, part2: 409.5 to 420.5, 429.5 to 440.5, 449.5 to 460.5, 469.5 to 480.5, 489.5 to 500.5, 509.5 to 520.5, 529.5 to 540.5, 549.5 to 560.5, 569.5 to 580.5, 589.5 to 600.5, 609.5 to 620.5, 629.5 to 640.5, 649.5 to 660.5, 669.5 to 680.5, 689.5 to 700.5, 709.5 to 720.5, 729.5 to 740.5, 749.5 to 760.5, 769.5 to 780.5, 789.5 to 800.5, 829.5 to 860.5, 899.5 to 940.5, 999.5 to 1060.5, 1129.5 to 1200.5. The following MS2 analysis was performed at 30,000 resolution, with an AGC target of 1e6 and a maximum ion injection time of 50 ms.

MS Data Analysis Using Spectronaut and DIA-NN

Two hundred sixty-four DDA files for library generation were analyzed in Spectronaut (version 13.3.190902.43655) against an UniprotKB/Swiss-Prot mouse protein database (downloaded at 10 September, 2018, 16,935 reviewed protein sequences). The mass tolerance of precursor and fragment ions was dynamic as the default setting suggested. Carbamidomethyl (C) was set as a fixed modification and oxidation (M) as a variable modification. The false discovery rate cut-off for peptide, protein, and the peptide-spectrum match were all set as 0.01.

Raw files from PulseDIA analysis were analyzed by DIA-NN 1.7.17 in the "robust LC (high precision)" mode. We used the spectral library generated previously by Spectronaut with a filter criterion of removing "True" from the column "Excluded from assay" in the library. The parameters were set as below: peptide length: 5 to 30; precursor m/z: 400 to 1200; fragment ion m/z range: 100 to 1500; peptide and protein

false discovery rates: below 1%. MS1 mass accuracy, scan window size, and modifications were set as default. For the data generated from the four male mice, match-between-run was not performed, and the resulting report was stringently filtered at 0.01 Global.Q.Value and 0.01 Global.PG.Q.Value according to the user manual. For every 24 files of the nine paired organs, match-between-run was performed, and the resulting report was filtered at 0.01 Lib.Q.Value and 0.01 Lib.PG.Q.Value according to the user manual.

Statistical Analysis

Four Groups of Elevated Proteins—Tissue-enriched: at least five-fold higher than any other tissue; group-enriched: at least five-fold higher in a group of 2 to 7 tissues; enhanced: five-fold higher than the average across all other tissues; tissue-specific: for all the proteins expressed in only one organ.

Hierarchical Clustering of 41 Organs—Distance matrix computation of each organ was calculated by "dist" in R with method of "manhattan". Clustering was performed by "hclust" with method of "ward.D2".

The Differentially Expressed Proteins of G1, G2 and G3—Kruskal test was performed to identify the differentially expressed proteins (DEPs) in the three groups. Proteins with Benjamini-Hochberg (B.H.) adjusted p-value <0.001 were prioritized. "DunnTest" in FSA R package was then used to find out DEPs between every two groups based on the proteins filtered by the first step. Proteins with B.H. adjusted p-value <0.001, and |FC| >5 was prioritized.

DEPs of Immune Privileged Organs versus *Other Organs*—Nonparticipation test was used due to abnormal distribution of the data. Proteins with B.H. adjusted p-value <0.05 and |FC| >2 were prioritized. Organ selection criteria for "other organs": Immune organs and organs whose protein number was fewer than that of cornea [the organ with the lowest number of proteins identified in all immune privileged (IP) organs] were removed from "other organs", since immune organs may have a strong immune response to pull up the average of immune-related protein expression level, while organs with low protein identification number may pull down the average due to a large number of missing values. These two types of organs may introduce bias in DEPs exploration.

Comparison of Protein Data and mRNA Data—Spearman correlation coefficient (r) was calculated for log2-transformed protein and mRNA quantities using the "cor" function in R. SRatio of a pathway was defined as the number of proteins that have a significant correlation with their corresponding mRNAs divided by the total number of proteins detected in each pathway. "Ratio" was calculated as the number of detected proteins in a given pathway, divided by the total number of genes in a particular pathway.

High-Abundance Proteins—We ranked the averaged protein intensities in each tissue and selected those with an abundance which is higher than the 75% quartile plus 1.5 times the interquartile range as high-abundance proteins (HAPs). About 100 HAPs were detected for each tissue type. For the same proteins in different biological replicates of one organ, mean of MS signals is calculated as the intensity of the protein.

Proteomic Laterality Analysis—The t test (paired = T) was performed for proteomic data between the left side of organs and the right side of organs. Proteins with B.H. adjusted p-value <0.05 or p value <0.05 and |FC| >1.2 were prioritized.

RESULTS AND DISCUSSION

Generation of a Pan-Mouse Spectral Library Containing 12,320 Proteins

Thirty-six mouse organs were collected from three male and three female C57BL/6 mice. Proteins were extracted with PCT and digested with trypsin (11, 19). The resulting peptides were fractionated by SCX into six fractions and then analyzed by DDA-MS. Details of peptides and proteins identified in 36 organs are summarized in Figure 1*A*. The highest number of protein (8494) was identified in the intestine, while only 997 proteins were identified in the red blood cell. Altogether, this library contains 178,304 peptides, 12,195 protein groups, and 12,320 proteins.

Our DIA library is more comprehensive than the other spectral libraries reported previously (Fig. 1*B*). In 2016, a murine DIA library was reported with 66,857 unique peptides corresponding to 8240 unique proteins from six vascularized organs (20). MouseRefSWATH (17) published in 2020 is composed of transitions for 167,138 proteotypic peptides from 10,597 proteins. Another mouse SWATH library (18) published on the same year consists of 243,043 proteotypic peptides which correspond to 11,340 proteins. The library was built from extensive fractions of murine L929 cell line and nine tissues. Compared to the abovementioned libraries, ours include 1678 new proteins (supplemental Fig. S1*A*). Six hundred twenty-three of these proteins came from testis. The fur, the eye, the preputial gland, and the skin contributed 152, 133, 141, and 127 new proteins, respectively. The proteomes of these organs have not been reported previously. This highlights the importance of organ type diversity for comprehensive library generation. Our DIA spectral library provides the largest proteome coverage (72.6%), when compared with seven existing libraries of different multicellular organisms (17, 18, 21–24) (Fig. 1*C*).

To validate this library, we analyzed multiple organs from a female mouse by PulseDIA (supplemental Table S3) against the library, and the proteins from each organ were classified into four groups, including tissue-specific proteins, tissue-enriched proteins, group-enriched proteins, and tissue-enhanced proteins according to Uhlen *et al.* (25) (supplemental Fig. S1*B*). All the proteins belonging to four groups are called elevated proteins. Ingenuity pathway analysis (IPA) was then performed on each organ based on these proteins. Most of the elevated proteins were enriched in pathways related to organ functions (supplemental Fig. S1, *C–F*). For example, for immune organs, the pathways and functions enriched concerned immune cells and immune response, while for nervous system, they were related to development of neurons and signaling transduction. These results indicate that this library can be effectively applied to interpret DIA-MS data for different tissues.

Overview of DIA-Based Proteomic Profiling of 41 Organs in Four Male Mice

We collected 41 organs from four male mice and profiled their proteomes using PulseDIA and this library. This study analyzed all common tissue types, including several rarely studied organs such as the fur, lens, cornea, retina, and gall bladder. To ensure high quality of quantitative proteomic

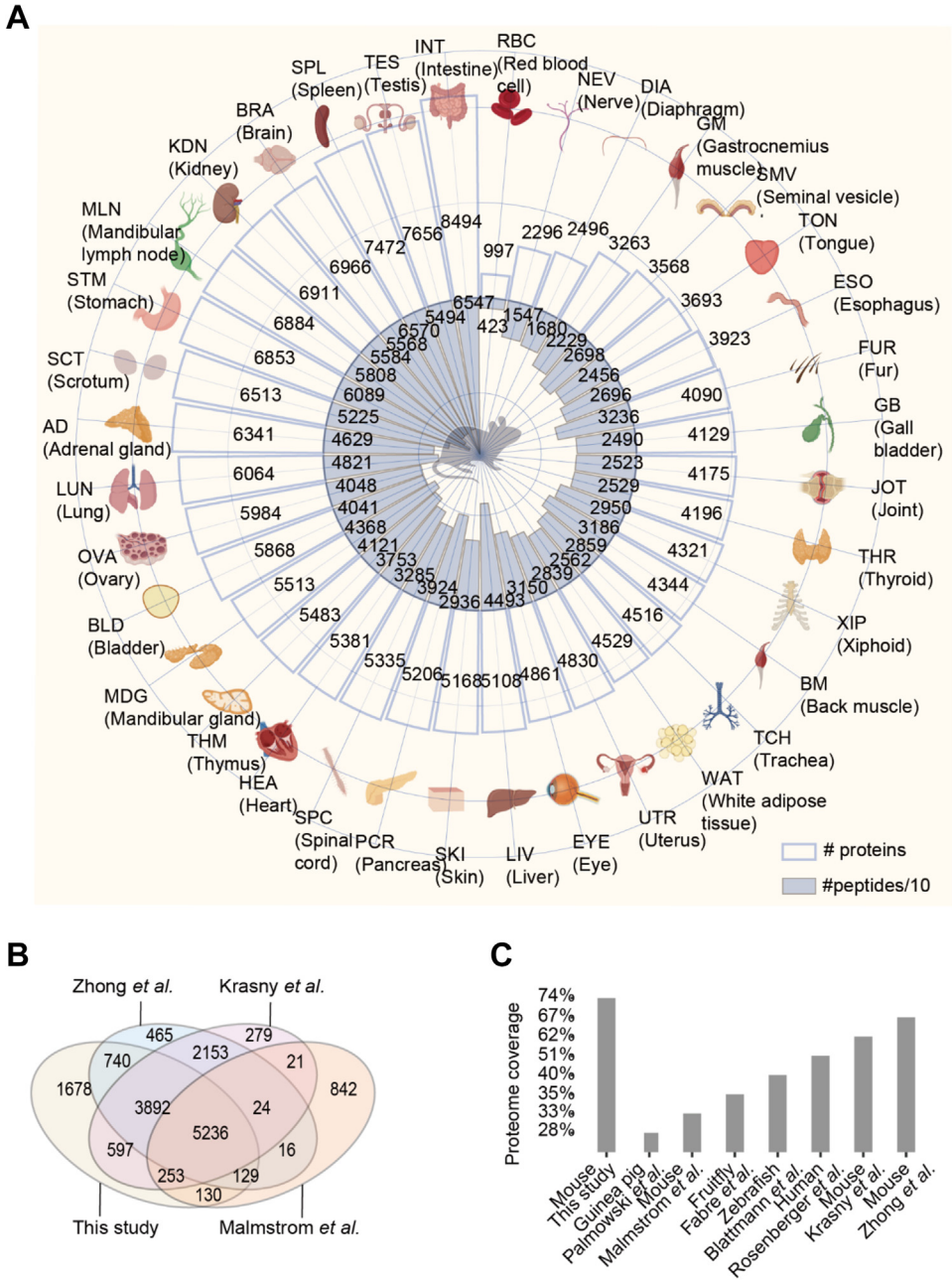

FIG. 1. **Overview of the spectral library.** *A*, numbers of peptides and proteins detected in 36 organs. *B*, our results compared to three other murine spectral libraries. *C*, proteome coverages of all published spectral libraries.

analysis, we included two types of quality control samples: one for assessing the quality of the sample preparation process as mouse liver samples, while the other for assessing the stability of MS data acquisition process as pool samples. We calculated coefficients of variation of the two types of quality control samples, which were both less than 10%, indicating the high quality of dataset (supplemental Fig. S2*A*).

Altogether we quantified 9388 proteins (supplemental Table S4) against a manually curated FASTA file with 16,935 entries, with over 6000 proteins quantified in most organs (supplemental Fig. S2*B*). All the DIA spectral libraries mentioned above are built against curated protein sequence FASTA file containing about 17,000 entries. This is different from several DDA-based proteomics studies which used much larger protein sequence FASTA files containing over 50,000 curated and predicted protein sequences (9, 10). All the proteins we reported here are curated proteins characterized with at least two peptides. Selected proteins of critical

roles are supported by manually inspected peak groups (supplemental Figs. S5 and S6).

The Nervous System and the Immune System Displayed the Most Distinct Proteome

We then computed the distance among different organs based on the quantitative proteomic data with a t-distributed stochastic neighbor embedding (t-SNE) analysis (Fig. 2*A*). We found that different tissues collected from the same organ clustered together, and different organs belonging to the same system also closely clustered, such as those belonging to the immune system, endocrine system, and reproductive organs, indicating that the thus quantified proteome is able to refect the sample origin. Tissues from the nervous system and the immune system clustered vastly distinct from other organs (Fig. 2*A*), indicating their unique proteomic profiles. It has also been reported that the brain tissues and muscle tissues clearly segregated from the others (9). Muscle tissues in our dataset, including the heart, the tongue, and the gastrocnemius muscle, were also distinct from other tissues in the t-SNE map, but not as significant as organs from the nervous system and the immune system.

All organs were then clustered into three groups as G1, G2, and G3 by hierarchical clustering (Fig. 2*B*), and the results were consistent with the t-SNE analysis, with organs of the nervous system and immune organs being the first to be distinguished from other organs (Fig. 2*B*). G1 is mainly composed of organs from the immune system, G2 contains organs from the nervous system, while the left organs are clustered together as G3. The types and locations of differentially expressed proteins (DEPs) between G1 and G3, G2 and G3 were summarized (supplemental Fig. S2, *C* and *D*). When comparing G1 with G3, most of the transcription regulators, transmembrane receptors, and proteins located in the nucleus were upregulated (supplemental Fig. S2*C*), suggesting active cell replication in the immune organs, which coincides with the fact that lymphocytes proliferate and differentiate in the immune organs. In comparison of G2 and G3, most of the G-protein coupled receptors, kinases, phosphatases, transporters, and proteins located in plasma membrane were upregulated in G2, while a large part of enzymes, peptidases showed higher expression level in organs of G3. The enrichment of kinases and phosphatases in the brain regions and retina sheds light on the importance of phosphorylation and dephosphorylation in the brain, which suggests active cell signaling in the nervous system.

IPA analysis (Fig. 2*C*) also revealed that many cell prolification-related pathways and immune-related pathways are activated in G1 compared to G3, such as cell cycle control of chromosomal replication, nucleotide excision repair (enhanced pathway), assembly of RNA polymerase 2 complex, and Th1 pathway. Testis was included in the G1 group; however, the pathways activated in the testis compared to G3 were mainly cell prolification–related pathways, with few immune-related pathways (data not shown), probably due to the immune privilege of the testis. PD-1, PD-L1 cancer immunotherapy pathway that inhibits immune responses is downregulated in G1 compared with G3. Pathways upregulated in G2 over G3 are mainly those related to neuronal cells or neural signaling, while pathways downregulated regard to coagulation and acute phase response pathway.

IP Organs Showed Distinct Immune-Related Protein Expression

IP organs, including the brain, the eye, the testis, and the pregnant uterus, are organs where foreign tissue grafts can survive. Although various mechanisms of immune privilege have been proposed, such as the presence of physical barriers like the blood–brain barrier (26), the blood–retina barrier (27), and the blood–testis barrier (28), as well as the absence of traditional lymphatics (26), etc., a systematical proteomic profiling of multiple IP organs is still lacking. We compared the proteomes of seven IP organs with several other organs (Fig. 3*A*) and found differences not only between IP organs and other organs but also within different IP organs. Based on a database of 847 proteins of the immune system (29), differential analysis was performed between IP organs and other organs, followed by pathway analysis by IPA (Fig. 3*B*). Acute phase response signaling, TNFR1 signaling, phagosome formation, NF-kB signaling, dendritic cell maturation, and other immune activation pathways were significantly downregulated in IP organs, while PD-1, PD-L1 cancer immunotherapy pathway which inhibits immune responses, and PTEN signaling that associates with tumor suppression (30) demonstrated significant elevation. It is reported that one of the multiple mechanisms under immune privilege is the immunosuppressive properties of local cells, such as the expression of TGFβ1-β3, IL-10, and activin A in the testis (28) and α-MSH, TGFβ2, and neuropeptide Y in the eye (27). Here, we shed light on PD-1, PD-L1 cancer immunotherapy pathway as a common immunosuppression pathway in seven IP organs. What's more, we found the activation of PTEN signaling, which may explain why these IP organs can avoid excessive tumor growth under immunosuppressive environment.

Major histocompatibility complex (MHC) plays an important role in immune rejection or immune privilege during transplantation (31). In mouse, MHC is called the H2 complex. Here, we found most of the IP organs had a smaller number and lower abundance of the H2 complex molecules than other tissues. This result is supported by a previous study, which found human pluripotent stem cells for cell-based transplantation therapy exhibited a lower expression of MHC molecules (31). Testis was found as an exception in these IP organs with relatively higher expression level of proteins of the H2 complex.

In addition, we compared the expression levels of proteins involved in acute phase response and complement system

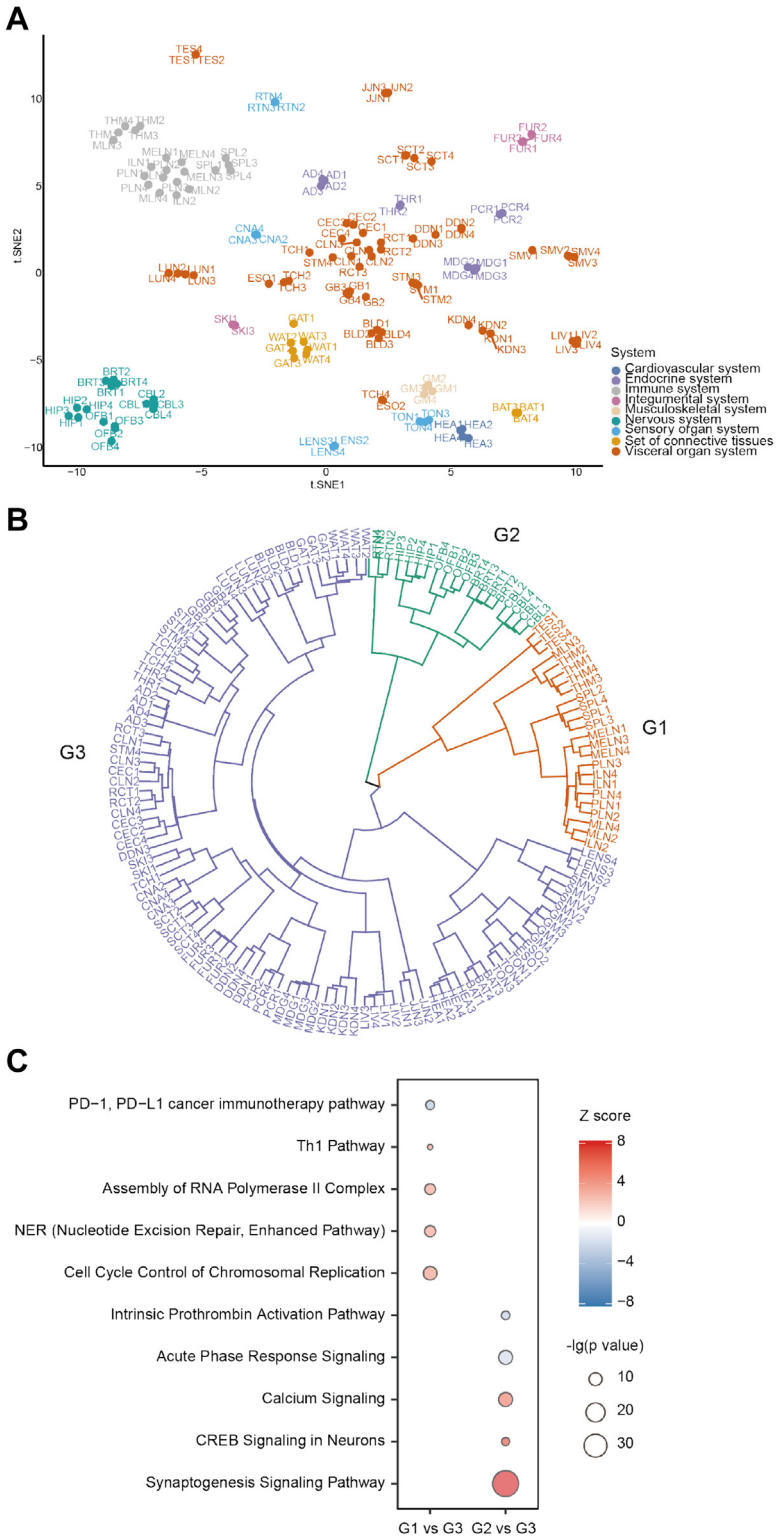

FIG. 2. **Proteomic clustering of three organ groups.** *A*, t-SNE map based on the mouse tissue proteome. *B*, hierarchical clustering of 41 organs into three groups. *C*, pathways enriched by the differentially expressed proteins in G1 *versus* G3 and G2 *versus* G3. t-SNE, t-distributed stochastic neighbor embedding.

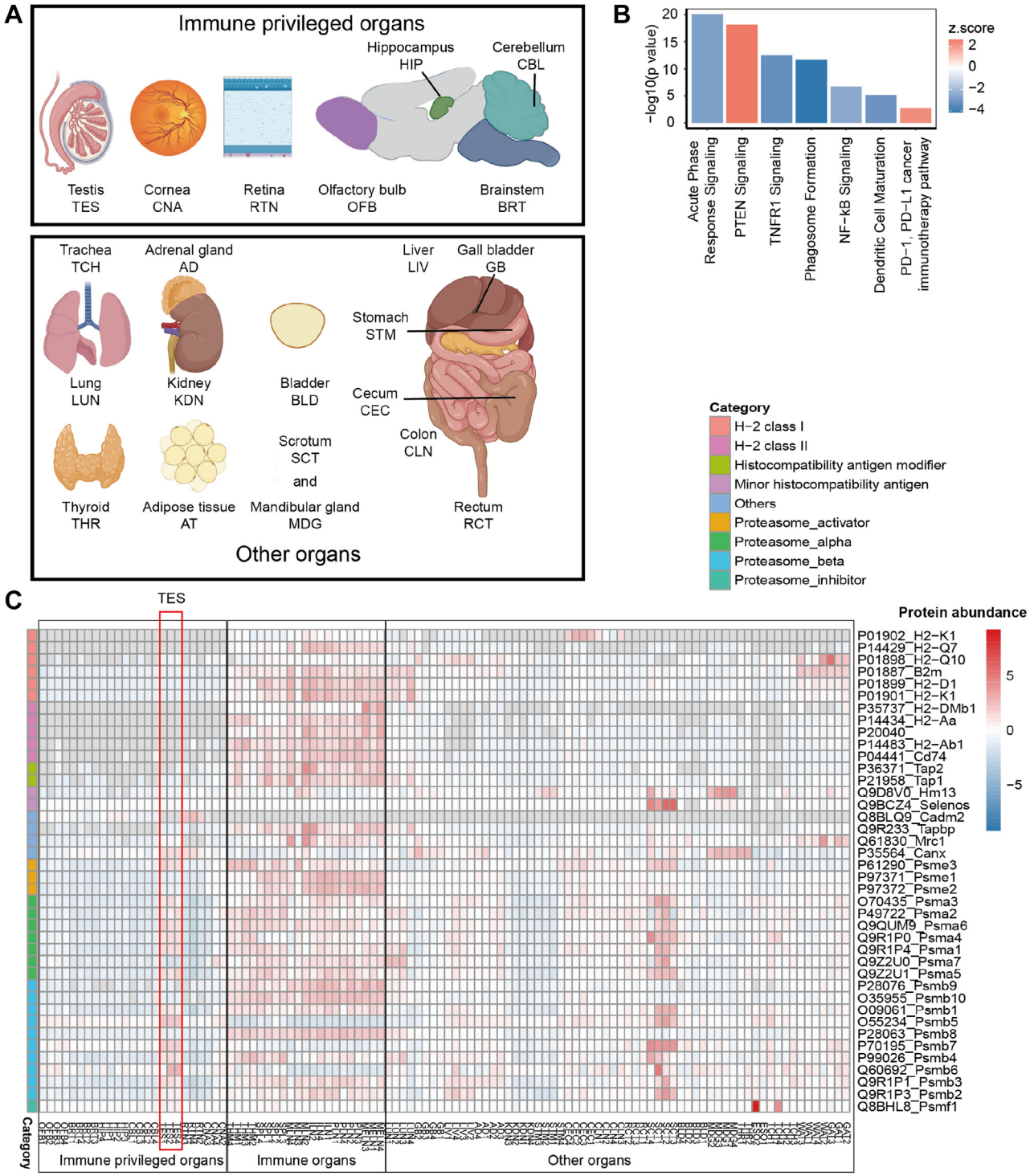

FIG. 3. **Immune privileged organs showed characteristic immune-related protein expression.** *A*, immune privileged organs and other organs included in DEPs analysis for pathway enrichment in *B*. *B*, pathways enriched in immune privileged organs *versus* other organs. *C*, the expression level of the H2 complex in 41 mouse organs.

(supplemental Fig. S3, *A* and *B*) in IP organs and other organs. In general, the abundance and number of these proteins were lower in IP organs, with the exception of the cornea. The cornea is the only organ directly contacting with the environment, which may explain its higher expression levels of these immune-related proteins. Our study is the first to systematically demonstrate the similarities and differences between multiple IP organs and other organs at the proteomic

level and will perhaps provide important hints for solving immune rejection after organ transplantation.

HAPs Performed Both Housekeeping and Tissue-Characteristic Functions

We defined HAPs as those with high MS intensities in a particular tissue. More details are provided in Experimental Procedures. Although the number of HAPs was about 2% of all proteins identified in a tissue (supplemental Fig. S4*A*), they constituted 40% to 90% of the intensity of all the detected proteins. With our proteomic methodology, 4000 ~ 7000 proteins were identified in most organs, while fewer than 3100 proteins were identified in the lens (n = 1683), seminal vesicle (n = 2778), and gastrocnemius muscle (n = 3100). In these three organs, the number of HAPs was fewer than 100, but they constituted more than 90% of the intensity of the detected proteome (Fig. 4*A*). This finding is a good complement to a recent study stating that 90% of the total protein abundance is made up by a relatively small fraction of proteins (10). While in the olfactory bulb (n = 6565), adrenal gland (n = 6570), and cecum (n = 6614), in which highest protein numbers were identified, the percentage of HAPs counts for about 50% of their protein intensity (Fig. 4*A*). Geiger *et al.* (9) reported that the abundance of top 100 proteins in muscle tissue [skeletal muscle (85%) and heart muscle (68%)] is higher than that in many other organs, also confirming the validity of our data [gastrocnemius muscle (92%) and heart muscle (82%)].

We classified the HAPs into two categories: for proteins identified as HAPs in more than 20 organs, we defined it as ubiquitous HAPs (n = 39) (Fig. 4, *B* and *C*) and for proteins identified as HAPs in fewer than five organs, we called it tissue-characteristic HAPs (n = 620) (Fig. 4*B*). It has been reported that top 100 proteins in each organ include metabolic enzymes, cytoskeletal proteins, ribosomal proteins, histones, albumin, and globins (9). These protein categories are consistent with the composition of ubiquitous HAPs in our dataset, which are also frequently used as internal standards for Western blotting (Fig. 4*C*).

Among the ubiquitous HAPs, we found peroxiredoxin-1, a major enzyme involved in cell protection against oxidative stress by detoxifying peroxides, suggesting critical roles of cell protection against oxidative stress in these organs. To further explore the importance of antioxidant protection, we explored the expression of other antioxidant-related proteins. Gstp, Gstm1, Gstm2, Prdx6, and Txn are also found to be highly abundant in more than ten organs, which are mainly from the digestive system, such as the liver, gall bladder, and gastrointestinal tract (Fig. 4*D*). This finding implicates that digestive organ may act as a major site of antioxidant against pro-oxidants from diets (32) and highlights the significance and prevalence of antioxidant functions.

GO enrichment and pathway analysis were performed for tissue-characteristic HAPs. Most of the proteins are closely related to the physiological functions of their corresponding organs. For example, in the adrenal gland, the top enriched functions are glucocorticoid biosynthetic process and steroid biosynthetic process. In the brainstem, cerebellum, olfactory bulb, and hippocampus, the top enriched functions are related to synaptic vesicle cycle and nervous system development. In the cornea, the lens, and the retina, the top functions are related to eye development and visual perception (supplemental Table S5). Our data suggest that the physiological functions of these organs are likely executed by these tissue-characteristic HAPs.

Most of Tissue-Specific Proteins Were Present in the Testis

Tissue-specific proteins are those detected in all biological replicates of an organ but not in any other organs, and we found that most of the tissue-specific proteins were presented in the testis (78 in 112) (supplemental Fig. S4*D*). Gprl1 and Sep14 have been reported as testis-specific proteins (33, 34), which supports our results. Manually inspected peak groups for these two proteins are provided in supplemental Fig. S5, *A–E*. We also found some novel tissue-specific proteins, such as Allc and Prs46 in the testis, with chromatographic evidence of peak groups (supplemental Fig. S6, *A–F*). We compared our results with the Geiger study (9) and found that the reported tissue-specific proteins were expressed at the highest levels in the corresponding organs in our dataset, for example, arginase 1 and glycogen synthase 2 in the liver, Cant1 in the intestine (corresponds to the colon, the jejunum, the cecum, the rectum, and the stomach in our dataset), Amacr in the kidney and the liver, and PAK1 in the neuronal tissues (corresponds to the four brain regions in our dataset) (supplemental Fig. S4*E*). However, probably because of inclusion of more organs and increased proteomics depth of this study, these proteins can be detected in other organs in our dataset as well.

Metabolism-Related Proteins Better Correlated With Their Transcripts Than Those in the Translational Process and Coagulation System

We compared our proteomic data with published mouse transcriptome data (35) by calculating the correlation between mRNAs and corresponding proteins for each organ based on the entire proteome and transcriptome. We computed SRatio to represent the relevance between proteins to their corresponding transcripts within a pathway (more details in Experimental Procedures) (supplemental Fig. S7*A*). Most pathways with SRatio multiplied by the ratio greater than 0.8, which indicates more than 80% of the proteins involved are highly correlated to mRNA expression, were involved in metabolism (supplemental Fig. S7*A*), including amino acid metabolism (supplemental Figs. S7*B* and S8*A*), ketogenesis, ketolysis, and fatty acid beta-oxidation, etc. For pathways with (1-SRatio) multiplied by the ratio greater than 0.4, which indicates more than 40% of the proteins involved are not significantly correlated to mRNA expression, were mainly

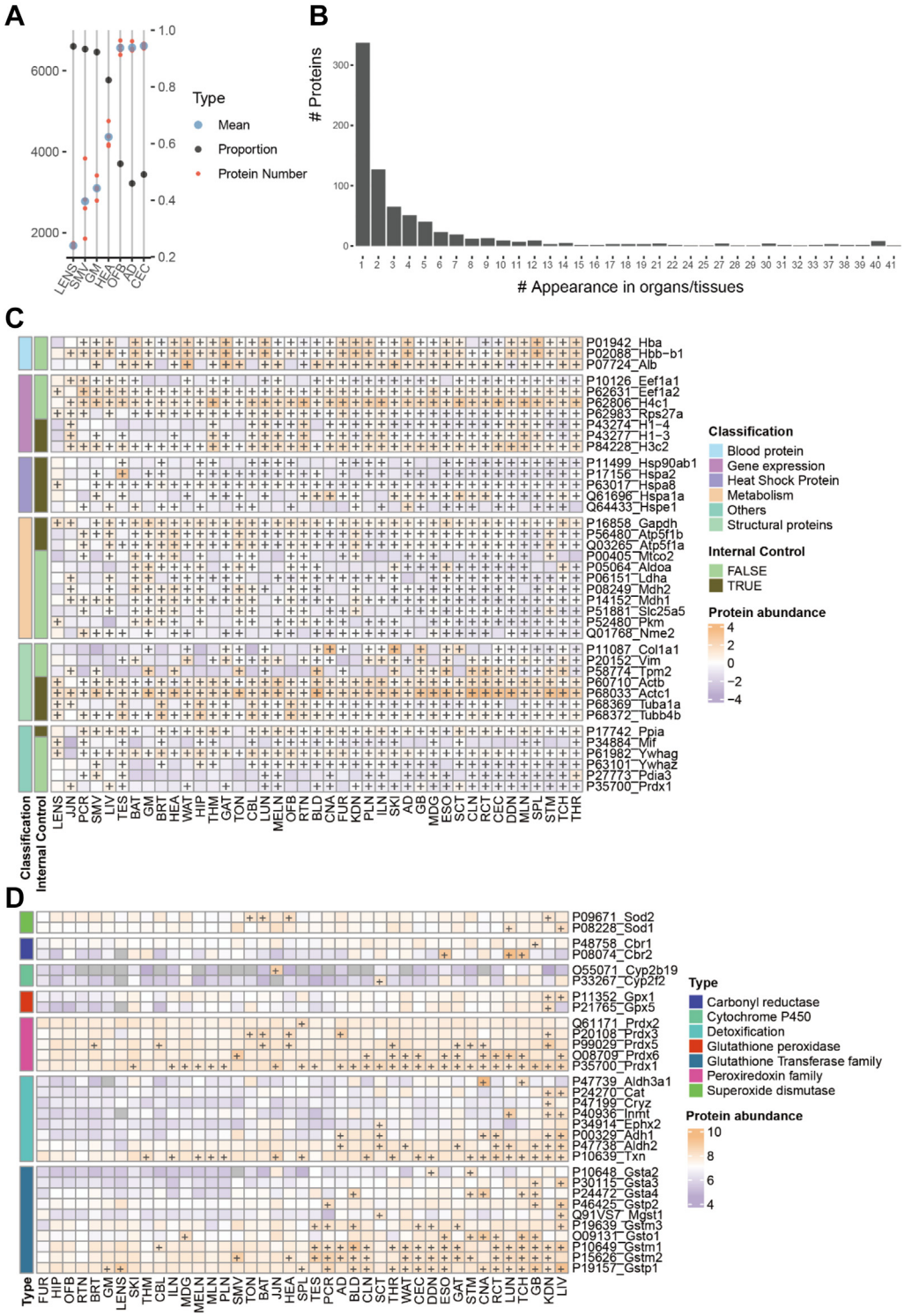

FIG. 4. **The HAPs in 41 mouse organs.** *A*, percentage of the cumulative abundances of the HAPs of the lens, the seminal vesicle, the gastrocnemius muscle, the heart, the olfactory bulb, the cecum, and the testis plotted against the number of proteins detected. *B*, organ distribution of HAPs. The number counts organs in which a protein is defined as HAP. *C*, the expression level of ubiquitous HAPs. "+" indicates this protein is defined as a HAP. *D*, the expression level of antioxidant-related proteins. HAPs, high-abundance proteins.

associated with translation process and coagulation system (supplemental Fig. S7*A*), including coagulation system (supplemental Fig. S8*B*), extrinsic prothrombin activation pathway, tRNA charging, and regulation of eIF2 signaling (supplemental Fig. S9*A*). Thus, higher degree of correlation between proteins and transcripts was observed for metabolic homeostasis-related pathways such as amino acid metabolism, while translation process and proteins involved in coagulation system exhibited weaker correlations. This phenomenon has also been observed in colorectal and ovarian cancer tissues (36, 37).

Proteomic Laterality in Multiple Organs Showed Elevated Antioxidant Enzymes in the Left Side of Body

We compared the DEPs in each of the nine paired organs of mice (Fig. 5*A*) and found that the adrenal glands exhibited highest number of DEPs between the left and right side, while hippocampus and olfactory bulb showed only one significantly different protein (supplemental Table S6 and supplemental Fig. S10). Interestingly, expression of four antioxidant-related enzymes was higher in the left side than in the right side of more than one organ (Fig. 5*B*). Vanin-1, the predominant isoform of pantetheinase (38), is reported to be upregulated under oxidative stress (39). Glutathione reductase and Cu/Zn superoxide dismutase are well-studied antioxidant enzymes for maintaining cellular redox homeostasis (40, 41). Hypoxia-inducible gene domain family member 1A is reported to lower cellular reactive oxygen species levels (42). In addition, the left kidney expresses higher level of a redox protein cytochrome b5 type B (Cyb5b) (Fig. 5*C*). The upregulation of these proteins may suggest a higher oxidative stress in left side of the adrenal gland, the testis, the mandibular lymph node, the thymus, the brainstem, the hippocampus, and the kidney.

Proteins related to organ functions or immune functions also showed left-right asymmetry (Fig. 5, *B* and *C*). Cd82 is a wide-spectrum tumor metastasis suppressor (43), and its expression was higher on the right side in the adrenal gland, kidney, and mandibular lymph node (Fig. 5*B*). Annexin A5 is widely used for detecting apoptotic process due to its ability to bind to phosphatidylserine by different imaging techniques (44), the expression level of which was higher in the right kidney (Fig. 5*C*). Serine protease inhibitor Kazal-type 2 is required for normal spermiogenesis as a strong inhibitor of acrosin (45). Its expression was found higher in the right testis. Neuronal precursor cell-expressed developmentally down-regulated protein 8 (Nedd8) is responsible for neddylation of target proteins. It is reported in the peri-infarct cortex after stroke and under neurodegenerative disorders, neddylation or Nedd8 is upregulated (46, 47). This protein was expressed at a higher level on the right side of the hippocampus. Aromatic-L-amino-acid decarboxylase and tryptophan 5-hydroxylase 2 are key enzymes for the generation of serotonin (48–50), an important neurotransmitter involving in multiple processes including mood control, sleep regulation, food intake, and sexual behavior (51). We observed their higher expressions on the right side of the cerebellum. Although interesting, these observations are mainly descriptive, deserving further investigation in future studies.

Comparison of Our Study to Two Previous Mouse Tissue Proteomics Studies

We compared our dataset with two previously published mouse proteome papers which analyzed at least 28 tissue types (supplemental Table S7). The Geiger *et al.* (9) paper investigated 28 organs, with samples from three animals pooled to one for data acquisition. The Giansanti *et al.* (10) paper included 15 mice, each contributing one to nine organs, making up a total of 41 organs, seven of which had one biological replicate. We collected 41 mouse organs, each with 3 to 4 biological replicates from four mice. The two papers used curated and predicted FASTA file with about 60,000 entries, while we used reviewed FASTA file with about 17,000 entries. We also removed single-peptide identifications, while the other two articles did not explicitly mention their protein identification strategy in the papers. The Geiger paper used SILAC for quantitative analysis, while Giansanti paper used iBAQ. Here, our study employed label-free DIA-MS. The Geiger paper reported the initial mouse whole-body proteomic atlas, and the Giansanti paper substantially extended these efforts by involving multiomics technologies, including proteome, phosphoproteome, and transcriptome, and collecting more tissue types and cell lines. Our study well complements these existing datasets by comparing nine paired organs between the left side and the right side. We analyzed multiple rarely approached tissue types and included four biological replicates for each DIA analysis, enabling more rigorous statistical analysis of protein expression among organs.

Limitations of This Study

Recent studies have shown the importance of female mammals in biomedical experiments, while sex bias still pervaded in a number of scientific biomedical fields (52). The proteomic data of female mice are relatively scarce in this paper, and the comparison of the female mouse with the male mouse is lacking due to a biased sample number. This issue deserves a new future study. Nevertheless, our dataset is a valuable resource for most male mouse-based studies.

CONCLUSION

Here, we report a comprehensive spectral library for targeted mass spectrometric analysis of over 12,000 mouse proteins and an in-depth proteomic atlas of 41 mouse tissues including multiple many previously rarely studied tissue types. The library comprises 1678 proteins which have not been reported in previous mouse spectral libraries. Our quantitative

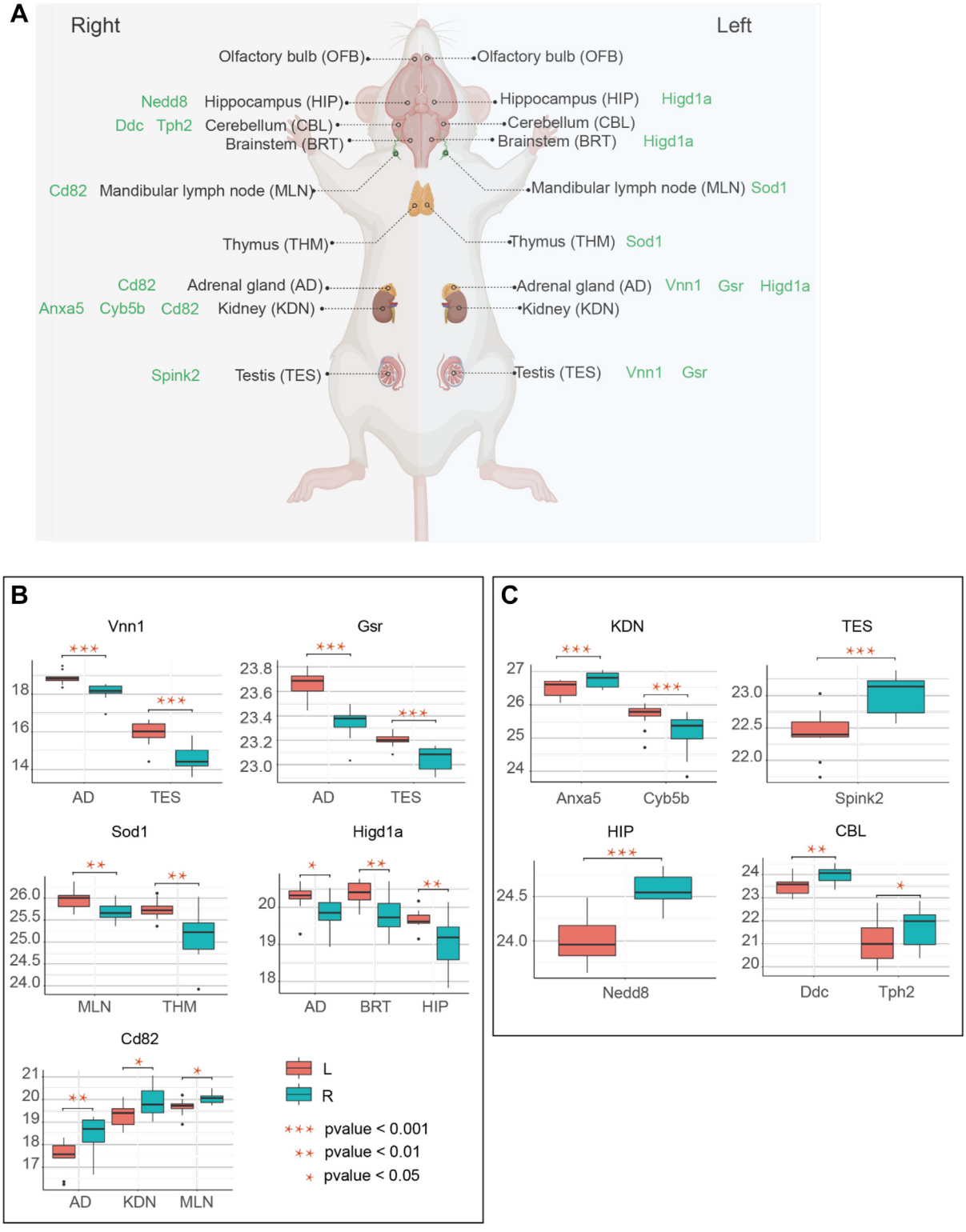

FIG. 5. **Protein laterality in nine mouse organs.** *A*, nine pairs of organs collected. Proteins with *green color* near the organs represent upregulated expression levels in the corresponding side. *B*, boxplot of DEPs detected in more than one organ. *C*, selected DEPs in organs with significant functions.

proteomics data suggest that the proteome of organs from the nervous system and immune system is most distinct from other organs and showed the distinctive proteomic features of IP organs, which might be helpful in addressing possible immune rejection after organ transplantation. We have also uncovered novel organ-specific proteins. Most tissue-specific proteins are detected in the testis. Metabolism-related proteins better correlate with their transcripts than those in the translational process and coagulation system. Finally, we also report that the left organs expressed higher level of antioxidant enzymes.

DATA AVAILABILITY

The proteomics data, the spectral library, and information for all proteins identified are deposited in ProteomeXchange Consortium (https://www.iprox.org/). Project ID: IPX0003625000.

Supplemental data—This article contains supplemental data.

Acknowledgments—This work is supported by grants from National Key R&D Program of China, China (No. 2021YFA1301602, 2020YFE0202200, 2021YFA1301603), the National Natural Science Foundation of China, China (81972492, 21904107), Zhejiang Provincial Natural Science Foundation, China for Distinguished Young Scholars (LR19C050001), Hangzhou Agriculture and Society Advancement Program (20190101A04), and Westlake Education Foundation, Tencent Foundation. We thank the Supercomputer Center of Westlake University for assistance in data storage and computation.

Author contributions—T. L., Y. X., and W. L. methodology; T. L., Y. X., Q. Z., and W. G. formal analysis; T. L., L. Q., and W. L. investigation; T. L. data curation; T. L. writing-original draft; T. L., L. Q., Y. Z., L. M., C. Z., and T. G. writing-review & editing; T. L. and Q. Z. visualization; Y. Z., L. M., C. Z., and T. G. supervision; Y. Z. and T. G. funding acquisition; T. G. conceptualization; T. G. resources; T. G. project administration.

Conflict of interest—T. G. and Y. Z. are shareholders of Westlake Omics Inc. Q. Z., W. G., and W. L. are employees of Westlake Omics Inc. The remaining authors declare no competing interests.

Abbreviations—The abbreviations used are: B.H., Benjamini-Hochberg; DDA, data-dependent acquisition; DEP, differentially expressed protein; DIA, data-independent acquisition; HAP, high-abundance protein; IP, immune privileged; IPA, ingenuity pathway analysis; MHC, major histocompatibility complex; MS, mass spectrometry; PCT, pressure cycling technology; SCX, strong cation exchange; SILAC, stable isotope labeling by amino acids in cell culture.

Received January 12, 2022, and in revised form, July 23, 2022
Published, MCPRO Papers in Press, September 2, 2022, https://doi.org/10.1016/j.mcpro.2022.100408

REFERENCES

1. Kolishovski, G., Lamoureux, A., Hale, P., Richardson, J. E., Recla, J. M., Adesanya, O., *et al*. (2019) The JAX Synteny Browser for mouse-human comparative genomics. *Mamm. Genome* **30**, 353–361
2. Sarsani, V. K., Raghupathy, N., Fiddes, I. T., Armstrong, J., Thibaud-Nissen, F., Zinder, O., *et al*. (2019) The genome of C57BL/6J "Eve", the mother of the laboratory mouse genome reference strain. *G3 (Bethesda)* **9**, 1795–1805
3. Tabula Muris, C. (2020) A single-cell transcriptomic atlas characterizes ageing tissues in the mouse. *Nature* **583**, 590–595
4. He, P., Williams, B. A., Trout, D., Marinov, G. K., Amrhein, H., Berghella, L., *et al*. (2020) The changing mouse embryo transcriptome at whole tissue and single-cell resolution. *Nature* **583**, 760–767
5. Aebersold, R., and Mann, M. (2016) Mass-spectrometric exploration of proteome structure and function. *Nature* **537**, 347–355
6. Kislinger, T., Cox, B., Kannan, A., Chung, C., Hu, P., Ignatchenko, A., *et al*. (2006) Global survey of organ and organelle protein expression in mouse: combined proteomic and transcriptomic profiling. *Cell* **125**, 173–186
7. Huttlin, E. L., Jedrychowski, M. P., Elias, J. E., Goswami, T., Rad, R., Beausoleil, S. A., *et al*. (2010) A tissue-specific atlas of mouse protein phosphorylation and expression. *Cell* **143**, 1174–1189
8. Skinnider, M. A., Scott, N. E., Prudova, A., Kerr, C. H., Stoynov, N., Stacey, R. G., *et al*. (2021) An atlas of protein-protein interactions across mouse tissues. *Cell* **184**, 4073–4089.e17
9. Geiger, T., Velic, A., Macek, B., Lundberg, E., Kampf, C., Nagaraj, N., *et al*. (2013) Initial quantitative proteomic map of 28 mouse tissues using the SILAC mouse. *Mol. Cell. Proteomics* **12**, 1709–1722
10. Giansanti, P., Samaras, P., Bian, Y., Meng, C., Coluccio, A., Frejno, M., *et al*. (2022) Mass spectrometry-based draft of the mouse proteome. *Nat. Methods* **19**, 803–811
11. Guo, T., Kouvonen, P., Koh, C. C., Gillet, L. C., Wolski, W. E., Röst, H. L., *et al*. (2015) Rapid mass spectrometric conversion of tissue biopsy samples into permanent quantitative digital proteome maps. *Nat. Med.* **21**, 407–413
12. Zhang, F., Ge, W., Ruan, G., Cai, X., and Guo, T. (2020) Data-independent acquisition mass spectrometry-based proteomics and software tools: a glimpse in 2020. *Proteomics* **20**, e1900276
13. Cai, X., Ge, W., Yi, X., Sun, R., Zhu, J., Lu, C., *et al*. (2021) PulseDIA: data-independent acquisition mass spectrometry using multi-injection pulsed gas-phase fractionation. *J. Proteome Res.* **20**, 279–288
14. Schubert, O. T., Gillet, L. C., Collins, B. C., Navarro, P., Rosenberger, G., Wolski, W. E., *et al*. (2015) Building high-quality assay libraries for targeted analysis of SWATH MS data. *Nat. Protoc.* **10**, 426–441
15. Zhu, T., Zhu, Y., Xuan, Y., Gao, H., Cai, X., Piersma, S. R., *et al*. (2020) DPHL: a DIA pan-human protein mass spectrometry library for robust biomarker discovery. *Genomics Proteomics Bioinformatics* **18**, 104–119
16. Ge, W., Liang, X., Zhang, F., Hu, Y., Xu, L., Xiang, N., *et al*. (2021) Computational optimization of spectral library size improves DIA-MS proteome coverage and applications to 15 tumors. *J. Proteome Res.* **20**, 5392–5401
17. Krasny, L., Bland, P., Burns, J., Lima, N. C., Harrison, P. T., Pacini, L., *et al*. (2020) A mouse SWATH-mass spectrometry reference spectral library enables deconvolution of species-specific proteomic alterations in human tumour xenografts. *Dis. Model. Mech.* **13**, dmm044586
18. Zhong, C. Q., Wu, J., Qiu, X., Chen, X., Xie, C., and Han, J. (2020) Generation of a murine SWATH-MS spectral library to quantify more than 11, 000 proteins. *Sci. Data* **7**, 104
19. Gao, H., Zhang, F., Liang, S., Zhang, Q., Lyu, M., Qian, L., *et al*. (2020) Accelerated lysis and proteolytic digestion of biopsy-level fresh-frozen and FFPE tissue samples using pressure cycling technology. *J. Proteome Res.* **19**, 1982–1990

20. Malmström, E., Kilsgård, O., Hauri, S., Smeds, E., Herwald, H., Malmström, L., *et al*. (2016) Large-scale inference of protein tissue origin in gram-positive sepsis plasma using quantitative targeted proteomics. *Nat. Commun.* **7**, 10261
21. Palmowski, P., Watson, R., Europe-Finner, G. N., Karolczak-Bayatti, M., Porter, A., Treumann, A., *et al*. (2019) The generation of a comprehensive spectral library for the analysis of the Guinea pig proteome by SWATH-MS. *Proteomics* **19**, e1900156
22. Blattmann, P., Stutz, V., Lizzo, G., Richard, J., Gut, P., and Aebersold, R. (2019) Generation of a zebrafish SWATH-MS spectral library to quantify 10,000 proteins. *Sci. Data* **6**, 190011
23. Rosenberger, G., Koh, C. C., Guo, T., Röst, H. L., Kouvonen, P., Collins, B. C., *et al*. (2014) A repository of assays to quantify 10,000 human proteins by SWATH-MS. *Sci. Data* **1**, 140031
24. Fabre, B., Korona, D., Mata, C. I., Parsons, H. T., Deery, M. J., Hertog, M. L. A. T. M., *et al*. (2017) Spectral libraries for SWATH-MS assays for Drosophila melanogaster and Solanum lycopersicum. *Proteomics* **17**. https://doi.org/10.1002/pmic.201700216
25. Uhlén, M., Fagerberg, L., Hallström, B. M., Lindskog, C., Oksvold, P., Mardinoglu, A., *et al*. (2015) Proteomics. Tissue-based map of the human proteome. *Science* **347**, 1260419
26. Forrester, J. V., McMenamin, P. G., and Dando, S. J. (2018) CNS infection and immune privilege. *Nat. Rev. Neurosci.* **19**, 655–671
27. Taylor, A. W. (2016) Ocular immune privilege and transplantation. *Front. Immunol.* **7**, 37
28. Li, N., Wang, T., and Han, D. (2012) Structural, cellular and molecular aspects of immune privilege in the testis. *Front. Immunol.* **3**, 152
29. Ortutay, C., and Vihinen, M. (2006) Immunome: a reference set of genes and proteins for systems biology of the human immune system. *Cell Immunol.* **244**, 87–89
30. Keniry, M., and Parsons, R. (2008) The role of PTEN signaling perturbations in cancer and in targeted therapy. *Oncogene* **27**, 5477–5485
31. Chen, H. F., Yu, C. Y., Chen, M. J., Chou, S. H., Chiang, M. S., Chou, W. H., *et al*. (2015) Characteristic expression of major histocompatibility complex and immune privilege genes in human pluripotent stem cells and their derivatives. *Cell Transplant.* **24**, 845–864
32. Halliwell, B., Zhao, K., and Whiteman, M. (2000) The gastrointestinal tract: a major site of antioxidant action? *Free Radic. Res.* **33**, 819–830
33. Gibbs, G. M., Lo, J. C., Nixon, B., Jamsai, D., O'Connor, A. E., Rijal, S., *et al*. (2010) Glioma pathogenesis-related 1-like 1 is testis enriched, dynamically modified, and redistributed during male germ cell maturation and has a potential role in sperm-oocyte binding. *Endocrinology* **151**, 2331–2342
34. Shinoda, T., Ito, H., Sudo, K., Iwamoto, I., Morishita, R., and Nagata, K. (2010) Septin 14 is involved in cortical neuronal migration via interaction with Septin 4. *Mol. Biol. Cell* **21**, 1324–1334
35. Li, B., Qing, T., Zhu, J., Wen, Z., Yu, Y., Fukumura, R., *et al*. (2017) A comprehensive mouse transcriptomic BodyMap across 17 tissues by RNA-seq. *Sci. Rep.* **7**, 4200
36. Zhang, B., Wang, J., Wang, X., Zhu, J., Liu, Q., Shi, Z., *et al*. (2014) Proteogenomic characterization of human colon and rectal cancer. *Nature* **513**, 382–387
37. Zhang, H., Liu, T., Zhang, Z., Payne, S. H., Zhang, B., McDermott, J. E., *et al*. (2016) Integrated proteogenomic characterization of human high-grade serous ovarian cancer. *Cell* **166**, 755–765
38. Naquet, P., Pitari, G., Duprè, S., and Galland, F. (2014) Role of the Vnn1 pantetheinase in tissue tolerance to stress. *Biochem. Soc. Trans.* **42**, 1094–1100
39. Berruyer, C., Martin, F. M., Castellano, R., Macone, A., Malergue, F., Garrido-Urbani, S., *et al*. (2004) Vanin-1-/- mice exhibit a glutathione-mediated tissue resistance to oxidative stress. *Mol. Cell. Biol.* **24**, 7214–7224
40. Couto, N., Wood, J., and Barber, J. (2016) The role of glutathione reductase and related enzymes on cellular redox homoeostasis network. *Free Radic. Biol. Med.* **95**, 27–42
41. Montllor-Albalate, C., Kim, H., Thompson, A. E., Jonke, A. P., Torres, M. P., and Reddi, A. R. (2022) Sod1 integrates oxygen availability to redox regulate NADPH production and the thiol redoxome. *Proc. Natl. Acad. Sci. U. S. A.* **119**, e2023328119
42. Ameri, K., Jahangiri, A., Rajah, A. M., Tormos, K. V., Nagarajan, R., Pekmezci, M., *et al*. (2015) HIGD1A regulates oxygen consumption, ROS production, and AMPK activity during glucose deprivation to modulate cell survival and tumor growth. *Cell Rep.* **10**, 891–899
43. Liu, W. M., and Zhang, X. A. (2006) KAI1/CD82, a tumor metastasis suppressor. *Cancer Lett.* **240**, 183–194
44. Ntziachristos, V., Schellenberger, E. A., Ripoll, J., Yessayan, D., Graves, E., Bogdanov, A., *et al*. (2004) Visualization of antitumor treatment by means of fluorescence molecular tomography with an annexin V-Cy5.5 conjugate. *Proc. Natl. Acad. Sci. U. S. A.* **101**, 12294–12299
45. Lee, B., Park, I., Jin, S., Choi, H., Kwon, J. T., Kim, J., *et al*. (2011) Impaired spermatogenesis and fertility in mice carrying a mutation in the Spink2 gene expressed predominantly in testes. *J. Biol. Chem.* **286**, 29108–29117
46. Yu, H., Luo, H., Chang, L., Wang, S., Geng, X., Kang, L., *et al*. (2022) The NEDD8-activating enzyme inhibitor MLN4924 reduces ischemic brain injury in mice. *Proc. Natl. Acad. Sci. U. S. A.* **119**, e2111896119
47. Mori, F., Nishie, M., Piao, Y. S., Kito, K., Kamitani, T., Takahashi, H., *et al*. (2005) Accumulation of NEDD8 in neuronal and glial inclusions of neurodegenerative disorders. *Neuropathol. Appl. Neurobiol.* **31**, 53–61
48. Pearson, T. S., Gupta, N., San Sebastian, W., Imamura-Ching, J., Viehoever, A., Grijalvo-Perez, A., *et al*. (2021) Gene therapy for aromatic L-amino acid decarboxylase deficiency by MR-guided direct delivery of AAV2-AADC to midbrain dopaminergic neurons. *Nat. Commun.* **12**, 4251
49. Walther, D. J., Peter, J. U., Bashammakh, S., Hörtnagl, H., Voits, M., Fink, H., *et al*. (2003) Synthesis of serotonin by a second tryptophan hydroxylase isoform. *Science* **299**, 76
50. Zhang, X., Beaulieu, J. M., Sotnikova, T. D., Gainetdinov, R. R., and Caron, M. G. (2004) Tryptophan hydroxylase-2 controls brain serotonin synthesis. *Science* **305**, 217
51. Veenstra-VanderWeele, J., Anderson, G. M., and Cook, E. H., Jr. (2000) Pharmacogenetics and the serotonin system: initial studies and future directions. *Eur. J. Pharmacol.* **410**, 165–181
52. Beery, A. K., and Zucker, I. (2011) Sex bias in neuroscience and biomedical research. *Neurosci. Biobehav. Rev.* **35**, 565–572